Reduction of solar photovoltaic resources due to air pollution in China

Xiaoyuan Li[a], Fabian Wagner[b,c,d], Wei Peng[b,1], Junnan Yang[b], and Denise L. Mauzerall[a,b,2]

[a]Department of Civil and Environmental Engineering, Princeton University, Princeton, NJ 08544; [b]Woodrow Wilson School of Public and International Affairs, Princeton University, Princeton, NJ 08544; [c]Air Quality and Greenhouse Gases Program, International Institute for Applied Systems Analysis, A-2361 Laxenburg, Austria; and [d]Andlinger Center for Energy and the Environment, Princeton University, Princeton, NJ 08544

Edited by M. Granger Morgan, Carnegie Mellon University, Pittsburgh, PA, and approved September 27, 2017 (received for review June 26, 2017)

Solar photovoltaic (PV) electricity generation is expanding rapidly in China, with total capacity projected to be 400 GW by 2030. However, severe aerosol pollution over China reduces solar radiation reaching the surface. We estimate the aerosol impact on solar PV electricity generation at the provincial and regional grid levels in China. Our approach is to examine the 12-year (2003–2014) average reduction in point-of-array irradiance (POAI) caused by aerosols in the atmosphere. We apply satellite-derived surface irradiance data from the NASA Clouds and the Earth's Radiant Energy System (CERES) with a PV performance model (PVLIB-Python) to calculate the impact of aerosols and clouds on POAI. Our findings reveal that aerosols over northern and eastern China, the most polluted regions, reduce annual average POAI by up to 1.5 kWh/m^2 per day relative to pollution-free conditions, a decrease of up to 35%. Annual average reductions of POAI over both northern and eastern China are about 20–25%. We also evaluate the seasonal variability of the impact and find that aerosols in this region are as important as clouds in winter. Furthermore, we find that aerosols decrease electricity output of tracking PV systems more than those with fixed arrays: over eastern China, POAI is reduced by 21% for fixed systems at optimal angle and 34% for two-axis tracking systems. We conclude that PV system performance in northern and eastern China will benefit from improvements in air quality and will facilitate that improvement by providing emission-free electricity.

renewable energy | solar photovoltaic | aerosols | air pollution | China

Solar photovoltaic (PV), a renewable and clean energy source with no direct emissions of carbon dioxide or air pollutants during operation, has been expanding exponentially worldwide over the past two decades (1). This increasing penetration rate is mainly driven by decreasing manufacturing costs, government incentives, a desire to reduce air pollution emissions, and an increasing awareness of climate change as a long-term threat to human welfare (1, 2). In China, total capacity of solar PV quintupled from 8 to 43 GW between 2012 and 2015 (1, 3). This growing trend is expected to continue in the future, especially in China, as the Chinese Government aims to more than double the total installed capacity of PV to 110 GW by 2020 (4). The government goal for 2030 is to increase PV capacity to 400 GW, thus providing ∼10% of total electricity demand and helping to fulfill China's commitment at the 2015 Paris Climate Conference to produce 20% of primary energy from nonfossil sources by 2030 (5–8). Improving solar PV material for high conversion efficiency, lowering material and manufacturing costs, and continuing government incentives will be key drivers of PV expansion (9). In addition, it is also important to understand the spatial distribution and temporal variability of surface solar resources to optimize efficient use of PV and reduce impacts of PV grid integration (10, 11).

The diurnal solar cycle and clouds have long been considered the major factors modulating surface solar radiation. However, atmospheric aerosols also attenuate solar radiation by scattering and absorbing sunlight before it reaches the surface (12, 13) but have not previously been considered when evaluating the productivity of solar PV panels. Here, we quantitatively evaluate the reduction in PV generation resulting from atmospheric aerosols. As developing countries with severe air pollution, such as China and India, rapidly expand solar PV in their power sectors (7, 14), attenuation by aerosols is often neglected in solar PV planning but can be an important factor to consider.

In fact, largely because of increasing aerosol concentration from anthropogenic emissions, previous studies have already reported a surface dimming trend in China since 2000 based on quality-controlled surface solar radiation data (15–17). An increase in absorbing aerosols (e.g., black carbon and brown organic aerosols) was found to have a considerable contribution to this dimming trend (18–20). A recent study in ref. 21 attributed 20% of the average solar dimming in China to aerosols, with contributions as large as 40% when wind speeds are very low. The reduction in surface solar radiation by aerosols also affects the solar energy available for solar electricity generation. Furthermore, aerosol concentrations also have strong seasonal variations (22). Intermittency caused by clouds has been widely recognized and studied in Europe and the United States, where solar PV was first developed and utilized for electricity generation (23–25). As an important factor, understanding the seasonal variability of reduction in PV generation caused by aerosols can facilitate PV grid integration in a way that better accounts for resource variability.

However, the link between aerosol-induced solar dimming and PV resources has not been previously studied quantitatively. Here, we quantify the impact of aerosols on PV electricity generation in China to understand its impact on generation efficiency. In addition, aerosols have a heterogeneous spatial distribution, with higher concentrations over eastern China and

Significance

Enormous growth in solar photovoltaic (PV) electricity generation in China is planned, with a goal to provide 10% of total electricity demand by 2030. However, over much of China, aerosol pollution scatters and absorbs sunlight, significantly reducing surface solar radiation suitable for PV electricity generation. We evaluate the impact of aerosols on PV generation and find aerosol-related annual average reductions in eastern China to be more than 20%. In winter, aerosols have comparable impacts to clouds over eastern provinces. Improving air quality in China would increase efficiency of solar PV generation. As a positive feedback, increased PV efficiency and deployment would further reduce air pollutant emissions as well.

Author contributions: X.L., F.W., W.P., J.Y., and D.L.M. designed research; X.L. performed research; X.L. contributed new reagents/analytic tools; X.L., F.W., and D.L.M. analyzed data; and X.L. and D.L.M. wrote the paper.

The authors declare no conflict of interest.

This article is a PNAS Direct Submission.

[1]Present address: Belfer Center for Science and International Affairs, Harvard Kennedy School of Government, Cambridge, MA 02138.

[2]To whom correspondence should be addressed. Email: mauzeral@princeton.edu.

This article contains supporting information online at www.pnas.org/lookup/suppl/doi:10.1073/pnas.1711462114/-/DCSupplemental.

lower levels in the west. This implies a larger reduction in PV generation caused by aerosols over the populated and industrialized eastern China, where electricity demand is high. Our findings can contribute to future work that weighs the relative importance of transmission costs vs. increased generation when PV is deployed in remote clean areas and to work that quantifies the multiple benefits that air quality improvements have.

In this study, aerosol impacts on solar PV generation are quantified. We apply the PVLIB-Python model, a PV performance tool, to calculate point-of-array irradiance (POAI) incident on a PV panel. For model input, we use satellite-derived surface irradiance data from the NASA Clouds and the Earth's Radiant Energy System (CERES)-SYN1deg for POAI. (Details of the model and datasets are described in *Materials and Methods*.) We use the CERES irradiance data for multiple aerosol and cloud conditions to compare the impact of aerosols vs. clouds on POAI. A total of nine experiments are designed to explore the implications of three PV panel settings [(*i*) fixed angle, (*ii*) one-axis tracking (One-T), and (*iii*) two-axis tracking (Two-T)] and three atmospheric conditions [(*i*) all sky (AS), which includes both realistic aerosols and clouds; (*ii*) clear sky (CS), which does not include cloud but includes aerosols; and (*iii*) all sky without aerosol (NA), which does not include aerosols but includes clouds]. The experiments span 2003–2014 (12 y) over a region (10° N to 55° N, 75 °E to 145° E) covering all of China with a spatial resolution of 1° latitude × 1° longitude. POAI at each grid cell is simulated at a 3-h temporal resolution in the PVLIB-Python model. The 3-h mean values are averaged over the 2003–2014 time period to calculate the average POAI within a grid cell. Details of the nine experiments are described in Tables 1 and 2. The baseline POAI directly results from the AS experiments. The impact that aerosols have on POAI is calculated by $POAI_{NA} - POAI_{AS}$ (NA minus AS) and likewise, for clouds ($POAI_{CS} - POAI_{AS}$; CS minus AS).

Using the above experiments and analyses, we first evaluate the aerosol optical depth (AOD) used by the CERES-SYN dataset to calculate aerosol radiative effects and then examine (*i*) a reference level of aerosol radiative effects obtained from the 12-y (2003–2014) average impact of aerosols on surface solar resources in China at both the provincial and electricity grid levels for fixed panels (FIXs) at the optimal angle to maximize received irradiance over the course of the year; (*ii*) the seasonal variability of aerosol impacts and a comparison with the impact of clouds; and (*iii*) the influence of panel settings (i.e., fixed or tracking systems) on the effect of aerosols on solar PV generation. Finally, we discuss the PV deployment and policy implications of our findings.

Evaluation of AODs

This study relies on satellite-derived surface solar irradiance to calculate baseline solar resources, aerosol, and cloud effects. The surface solar irradiance in CERES-SYN1deg is derived from the observed top of the atmosphere irradiance and the atmospheric extinction effects primarily determined by aerosol types, AOD, cloud fraction, and cloud optical depth. Among these factors, AOD is the most important variable in our analysis of aerosol effects on solar resource availability. AOD is a measure of solar radiation extinction by aerosols in the atmosphere. Ground-measured AODs are more accurate than satellite-measured AODs, because satellite retrievals heavily depend on air mass factor and surface albedo corrections, which add extra uncertainties. However, surface measurements are sparse, and satellite-measured AODs provide a more complete spatial coverage over China. Here, we evaluate the satellite AODs used in the CERES-SYN1deg dataset with ground-based observations over China.

CERES-SYN1deg applies AODs from the Moderate Resolution Imaging Spectroradiometer (MODIS), with missing values filled in by the Model for Atmospheric Transport and Chemistry (MATCH), to calculate the effects of aerosols on surface irradiances (26). MODIS AODs have been evaluated both at the global scale (27) and in various regions of China (28, 29) over specific time periods using observations from the Aerosol Robotic Network (AERONET). However, MODIS aerosol climatology has not been extensively evaluated in China during our evaluation period. This study aims to quantify the 12-y (2003–2014) average impacts from aerosols on surface irradiances for PV generation in China. Therefore, we evaluate the climatology of monthly mean AODs in CERES-SYN1deg (average from 2003 to 2013) against the ground-based observations from the China Remote Sensing Network (CARSNET; averaged from 2002 to 2013) at 50 sites in China.

Compared with CARSNET, AODs used by CERES-SYN1deg have mean biases less than 0.1 and small rms errors (RMSEs) over most sites in China (*SI Appendix*, Fig. S1). There is higher agreement over the very northern part of China and southern China compared with other regions. Over eastern China, most sites have biases over 0.1, and some are up to 0.5. This is mainly because the baseline AODs are higher in polluted eastern China, making the percentage bias similar to other regions. High biases (>0.5) occur at remote and rural sites, like Mt. Tai, Dongtan, and Changde, which are close to heavily polluted urban areas. This is because AODs used by CERES-SYN1deg represent the average AOD of a 1° × 1° grid box, which mixes in the higher AOD from neighboring urban areas. For example, Dongtan (a rural site) and Pudong (an urban site in Shanghai), measured separately in CARSNET, are very close to each other (less than 30 km apart) and are represented by one grid box in CERES-SYN1deg. The CERES AOD is much closer in value to measurement in Pudong, because this grid box contains a large urban area and thus, significant contributions from urban aerosols. Negative biases higher than −0.2 occur at two urban sites (Benxi and Lanzhou) and one desert site (Tazhong). The underestimation at Benxi and Lanzhou are likely caused by the relatively low AOD in the vicinity. The grid boxes that contain those sites are dominated by rural areas. Therefore, CERES AODs, averaged over each box, are much lower than the observations at these urban locations. The bias at Tazhong might be related to the underestimation of dust aerosol AODs over the Taklimakan Desert. We group all 50 sites into three categories (remote, rural, and urban) and perform statistical analysis on the AOD comparisons for each category (*SI Appendix*, Fig. S2). The 31 urban sites show the highest agreement, with very low mean bias (0.014; compared with the observation mean of 0.611) and high correlation (0.64). The 25 rural sites have the same correlation coefficient but higher bias (0.073; compared with the observation mean of 0.358). The four remote sites show the least agreement (62% bias and correlation coefficient of 0.5), because grid mean AODs in CERES-SYN1deg are higher than those at remote sites due to inclusion of some urban aerosols. In general, AOD climatology used in this study represents ground observations with relatively small bias (11%) and high correlation (0.71) over China.

Table 1. Design of experiments: Major scenarios

Name	Abbreviation	Descriptions
Fixed at optimal angle	FIX	The panel is tilted and fixed at the MacsLab angle (41), which maximizes the received irradiance year round
One-axis horizontal tracking	One-T	The panel rotates around a horizontal axis from east to west to track the sun throughout the day
Two-axis tracking	Two-T	The panel rotates around two axes so as to be perpendicular to direct irradiance at all times

Table 2. Design of experiments: Subscenarios

Name	Abbreviation	Include aerosol	Include clouds
All sky	AS	Yes	Yes
Clear sky	CS	Yes	No
All sky without aerosol	NA	No	Yes

2003–2014 Average Aerosol Impact

Baseline POAI over China features abundant insolation over western China and the northern part of northern China (Fig. 1). Over most of the west, the average daily POAI is more than 6 kWh/m^2 per day, with the largest value in Tibet (around 7 kWh/m^2 per day). Eastern China, with average daily POAI at only 3–4.5 kWh/m^2 per day, has 30–50% less insolation than western China. Our spatial distribution of solar resources agrees with previous studies (30) but has higher estimates, because we evaluate the maximum incident radiation for fixed optimally tilted panels rather than on a horizontal surface. This pattern of high solar resources in the west and north, while low in the east and south, is largely driven by surface elevation and cloud cover.

However, over eastern China, aerosols have especially strong impacts on POAI, which here, represents the maximum solar resources available to optimally tilted fixed panels (FIX). The 12-y annual average attenuation of POAI caused by aerosols is more than 1 kWh/m^2 per day over the most polluted regions in northern and eastern China (Fig. 2*A*). Compared with the baseline POAI, this reduction is more than 15% in eastern China and 25–35% over several northern and eastern provinces (Fig. 2*B*). In particular, aerosols decrease POAI by up to 35% over heavily polluted provinces, such as Shandong and Jiangsu. Western China, however, is affected less by anthropogenic aerosols than eastern China but affected more by dust aerosols. Average POAI reduction in western China is only 0.5 kWh/m^2 per day, about one-half of the attenuation in eastern China. Compared with the high baseline solar resources, the attenuation in western China is less than 10%, indicating a much smaller aerosol impact.

China's power transmission system consists of seven regional grids. Although power generation and electricity price decisions are made at the provincial level, provinces within each grid are interconnected, which enables intragrid electricity transmission. Therefore, within a grid, PV electricity could be transmitted from regions with relatively low to relatively high AOD, thus reducing the impact of aerosols on grid-scale PV integration. In addition to analysis at the provincial level, we, therefore, also analyze aerosol impacts at the grid level, assuming that PV electricity is transmitted efficiently within each grid. We take the average POAI over each electricity grid to represent the grid-level solar resources (Fig. 2*C*). The Eastern Grid (3 in Fig. 2*C*) has the largest reduction in POAI caused by aerosols (−0.83 kW/m^2 per day), and the Northern Grid (2 in Fig. 2*C*) has the second highest reduction (−0.73 kW/m^2 per day) (*SI Appendix*, Table S1). However, compared with the baseline resource of each grid, the Northern Grid (2 in Fig. 2*C*) is less impacted than the Eastern Grid (3 in Fig. 2*C*) and Central Grid (5 in Fig. 2*C*) (~13.7 vs. ~21.1 and ~15.9%, respectively). The Northern Grid is heavily influenced by aerosols over the eastern coastal region (Tianjin, Shandong, and Hebei), which has very high AOD, whereas the western inland part of the grid has relatively low AOD (31).

Aerosols Vs. Clouds

Clouds are the dominant factor modulating surface radiation and thus, causing the intermittency of solar electricity generation. Aerosols, however, induce attenuation of solar radiation with less variability but on average, are comparable with clouds in the Northern Grid and Eastern Grid during winter. Annual average effects of clouds are more than 10% larger than aerosols in all regions of China (*SI Appendix*, Fig. S3). In the Central Grid, Northeastern Grid, Southern Grid, and Northwestern Grid, monthly impacts from clouds are two to five times higher than those from aerosols. However, over the Northern Grid, the annual average impact of aerosols is closer to that of clouds: aerosols reduce the grid-average POAI by 14% compared with a 24% decrease because of clouds. By further analyzing the seasonality of the impacts (Fig. 3), we find that aerosols have a higher influence on POAI in winter than in summer, while clouds generally show the opposite pattern because of higher moisture levels and more numerous clouds in warm months. Higher monthly average impacts caused by aerosols than clouds have occurred in the Northern Grid (less frequently in the Eastern Grid), as indicated by the blue-shaded area overlapping the red area in Fig. 3. In this study, effects of clouds and aerosols are calculated separately using satellite observations. The aerosol indirect effect (i.e., increase of cloud amount caused by aerosols) is attributed to clouds rather than aerosols. Therefore, the real aerosol impact is larger than our calculations indicate, making it as important as clouds in modulating surface solar resource in winter over both the Northern Grid and the Eastern Grid.

Panel Settings and Aerosol Impacts

Aerosols decrease direct radiation and increase diffuse radiation, resulting in a net loss in radiation that reaches the surface (32). Most utility-scale solar farms deploy PV tracking systems to increase the utilization of direct sunlight (33) (One-T is applied to follow the diurnal change of the sun's position, while Two-T in addition follows the seasonal change of the sun's angle). As shown in Fig. 4, *Left*, the relatively clean western and the very northern parts of China benefit significantly from implementing tracking systems. In these regions, One-T increases the POAI by 1–1.5 kWh/m^2 per day. Two-T yields a stronger enhancement of 2–3 kWh/m^2 per day, a 40% increase in solar resources relative to FIX. However, this benefit is small (less than 10% increase) over eastern and southern China. Smaller benefits result from implementing tracking panels in eastern and southern China (where direct radiation is less than 35% of total radiation) than in other regions (*SI Appendix*, Fig. S4). This finding implies that, when deploying PV panels over southeastern China, FIX systems would capture most (about 90%) of the radiation, making the costly tracking systems less attractive. Nevertheless, installing

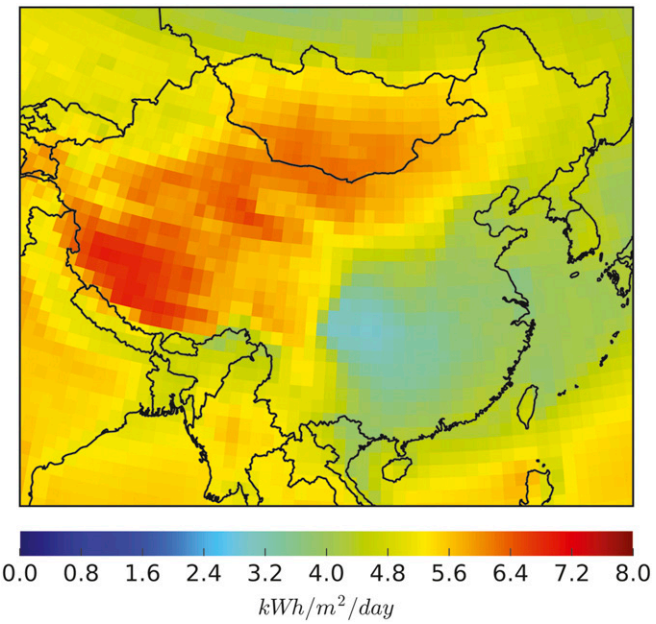

Fig. 1. Baseline mean (2003–2014) daily POAI over China for FIX at optimal angle.

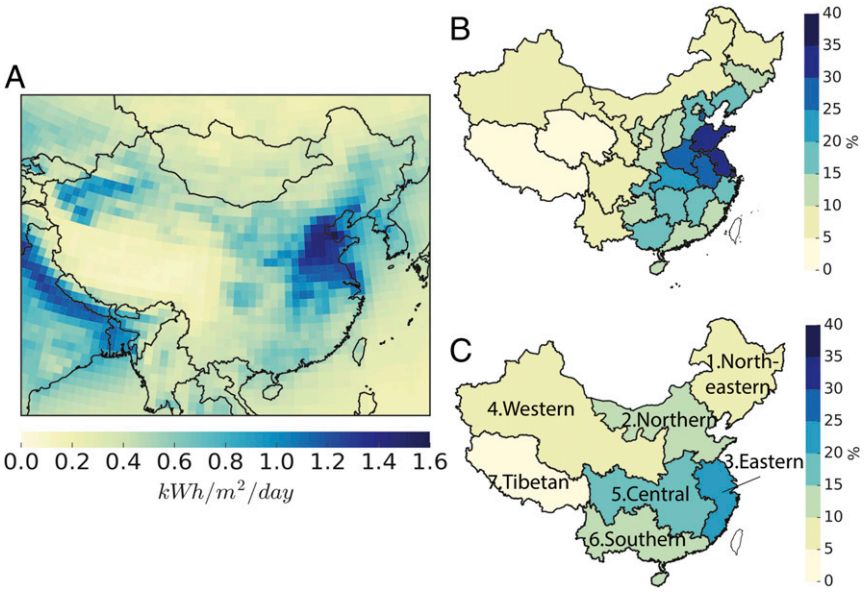

Fig. 2. Twelve-year average (2003–2014) effect of aerosols on surface POAI. (*A*) Reduction of POAI caused by aerosols. (*B*) Twelve-year average percentage reduction compared with baseline AS scenario for each province in China and (*C*) the same as *B* but for each electricity grid. The seven electricity grids in China include the Northeastern Grid (1), the Northern Grid (2), the Eastern Grid (3), the Northwestern Grid (4), the Central Grid (5), the Southern Grid (6), and the Tibetan Grid (7). High aerosol impacts are observed over the North China Plain (eastern China) and the Taklamakan Desert (western China) as well as the Indo-Gangetic Plain (northern India).

tracking systems in the resource-abundant clean western China could increase PV generation by up to 30%.

While One-T and Two-T enable PV panels to receive more radiation, aerosols also exert greater influence. Not only does the absolute impact of aerosols increase for more sophisticated tracking systems (Two-T > One-T > FIX), but the percentage change also becomes significantly larger. With tracking systems (One-T and Two-T), the angle between PV panels and direct surface solar radiation becomes smaller. Compared with FIX, tracking panels utilize more direct radiation. Aerosols attenuate direct radiation strongly by scattering and diffusing the light that passes through in all directions. However, they enhance diffuse radiation that reaches the surface by a smaller amount. Therefore, attenuation caused by aerosols on One-T and Two-T systems is larger than for FIX, leading to greater losses in PV productivity in highly polluted regions (Fig. 4, *Right*). In the Eastern Grid, aerosols reduce POAI by 21.1% in FIX, 29.3% in One-T, and up to 34.1% in Two-T. A similar increase in percentage impact of aerosols with more sophisticated tracking systems (Two-T > One-T > FIX) exists in other regions, especially in eastern grids.

Discussion and Conclusions

This study reveals that aerosol pollution in China greatly reduces surface solar PV resources. Especially high aerosol impacts exist over eastern China, where air pollution is severe and electricity demand is greatest. Aerosols reduce irradiance incident on optimally tilted fixed panels by up to 1.5 kWh/m^2 per day, incurring a high percentage decrease (25–35%) over polluted northern and eastern China. Clouds generally have a large influence in modulating surface radiation. However, during winter, aerosols can exert an influence as significant as clouds on solar resources over the Northern Grid and the Eastern Grid.

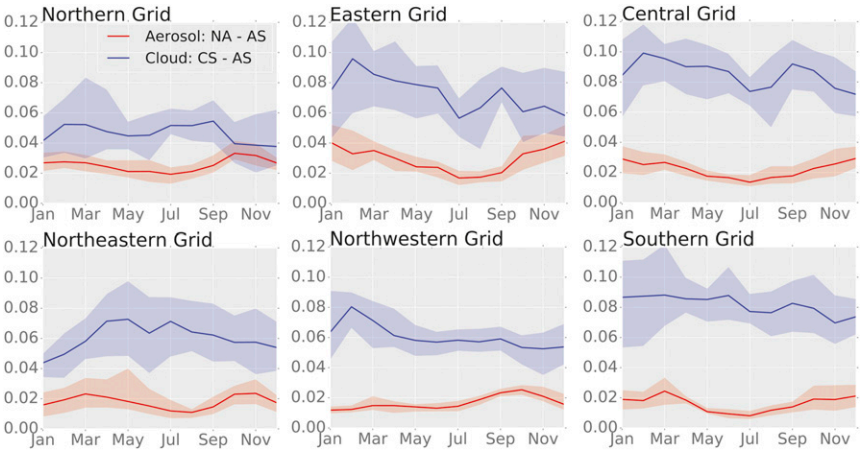

Fig. 3. Average monthly mean POAI decreases for 2003–2014 caused by aerosol and clouds over each electricity grid in China. Shaded area represents the monthly mean POAI 25th and 75th percentiles. Units are kilowatt hours per meter^2 per day.

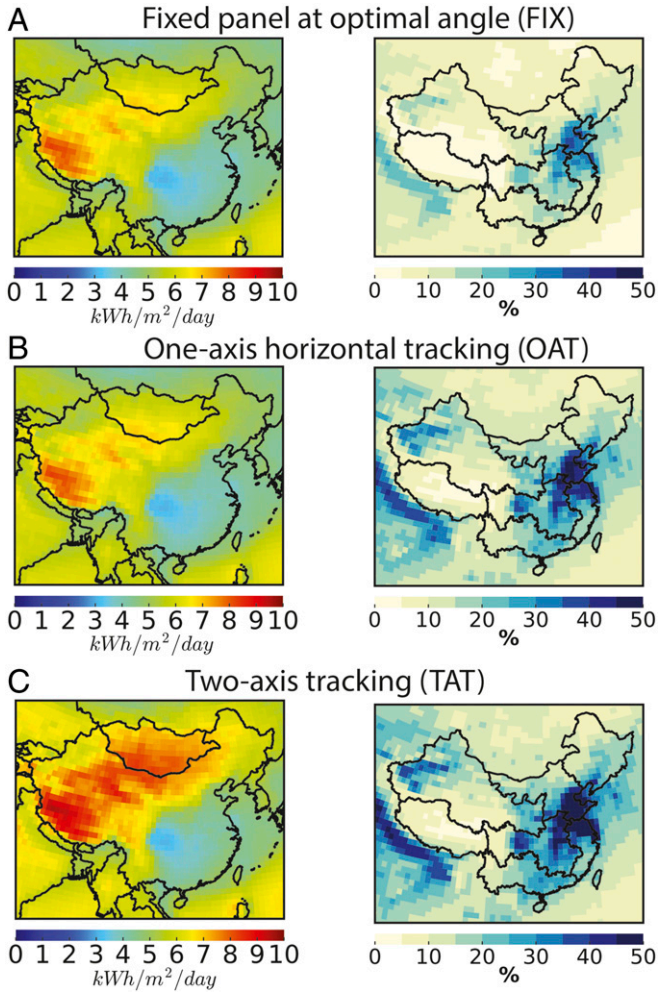

Fig. 4. Surface POAI (*Left*) and percentage reduction caused by aerosols (*Right*) for each type of PV panel setting: (*A*) FIX at optimal angle, (*B*) one-axis horizontal tracking (OAT), and (*C*) Two-T (TAT). Values of grid-level reduction can be found in *SI Appendix*, Table S1.

For tracking systems, which rely more on direct radiation (One-T or Two-T), aerosols decrease PV generation more than for fixed systems in terms of both absolute and percentage change. Aerosols over eastern China reduce the POAI by 21% for fixed systems and 34% for Two-T systems. However, aerosol impacts on tracking systems within a grid are heterogeneous, especially in the Northern Grid. The inland region of the Northern Grid (Western Inner Mongolia), which has abundant solar resources and much lower aerosol levels, can alleviate the impact of aerosols on Northern Grid PV generation. Therefore, intragrid transmission facilitates movement of PV electricity from clean to polluted areas within the grid. PV electricity generated using One-T or Two-T could be transmitted from a clean low-demand resource-abundant area to a more polluted high-demand area.

Our results indicate that air pollution mitigation has great potential to increase solar PV electricity generation in China. As the Chinese Government provides incentives for rooftop PV installation over the populated and urbanized eastern part of China, this benefit would be especially large (25–35% increase if aerosols were removed) in that region. Furthermore, utility-scale solar PV systems, usually installed with tracking systems that favor more direct radiation, would benefit even more from pollution mitigation, having greater absolute and percentage increases in PV generation when aerosols are removed.

This benefit would be especially large for concentrated solar power (CSP). As CSP can use only direct radiation, reduction of CSP generation caused by aerosols is even larger than reductions in PV generation. As shown in *SI Appendix*, Fig. S5, the largest impact would occur in the Eastern Grid, with an 80% decrease in direct POAI. Even in the less-polluted Western Grid, where CSP projects are being developed, the reduction is 30%. Western China has abundant solar resources, but there is significant heterogeneity in aerosol impacts on direct POAI within the region. Our finding facilitates future work on CSP project location planning and shows that aerosol loadings should be considered as an important factor.

Therefore, inclusion of solar resources as an important factor when conducting cost–benefit analysis of air pollution mitigation in China is justified. In addition, a higher penetration of clean and renewable energy, when displacing dirty coal generation, would not only result in less air pollution emissions but would also have a positive feedback and increase solar resources. This additional incentive may further encourage renewable energy deployment in China in addition to providing health and climate benefits. For a complete picture of the aerosol impacts on PV electricity generation, additional study is needed on the short-term variability of PV generation caused by air pollution episodes and the impact of attenuation by aerosols on the power system considering the temporal profiles of location-specific PV resources. Aerosol attenuation of POAI over northern India (the Indo-Gangetic Plain) is as substantial as over northern China. Our follow-up project analyzes global aerosol impacts on PV electricity generation with a focus on this region.

Materials and Methods

Solar PV System Performance Model—PVLIB-Python. PVLIB-Python, version 0.3.3, is an open source toolbox to perform advanced data analysis and research for PV system performance modeling and operations (34). PVLIB-Python can be applied to calculate the total output power from a solar PV system using observed irradiance and weather data (detailed below). Recent model development and improvements allow the performance modeling of the entire PV system, including specific PV module and inverter model characteristics at user-defined times and locations (35, 36). The model takes input of typical or measured weather and radiation data and provides the end product as the ac power output. This study leverages the flexibility of the open source model and applies it to calculate the effective irradiance incident on PV panels. In addition, we have developed a wrapper to enable parallel computing using the PVLIB-Python model, which increases the computing efficiency when applying calculations for a large number of grid point locations and time steps.

Aerosol, Clouds, and Meteorology Data. This study applies globally gridded (1° latitude × 1° longitude) observational data for radiation from the NASA CERES-SYN1deg Edition3A. Detailed information regarding the dataset is shown in *SI Appendix*, Table S2. The NASA CERES-SYN1deg provides 3-h average surface direct and diffuse irradiance globally at a resolution of 1° latitude × 1° longitude. These data are computed using the Langley Fu–Liou radiative transfer model calculations constrained by aerosol, cloud, and atmospheric (e.g., profile of temperature, pressure, water vapor, ozone, etc.) data. AODs over China are retrieved from MODIS and assimilated using the MATCH model for aerosol properties and vertical profiles at daily temporal resolution. Cloud properties are derived from MODIS and five geostationary satellites imagers (37, 38). A total of six satellites provide cloud data for China. Two are located at a longitude of ~63° E (Meteosat-5 and Meteosat-7), and four are located at ~140° E [Geostationary Meteorological Satellite-5, Geostationary Operational Environmental Satellite 9 (GOES-9), Multi-Functional Transport Satellite-1R (MTSAT-1R), and MTSAT-2]. Surface shortwave irradiance in the CERES-SYN1deg dataset has been evaluated in ref. 26 with observations at 37 globally distributed land sites (however, only one site is located in China at Xianghe near Beijing) from the Baseline Surface Radiation Network, the Global Monitoring Division, and Atmospheric Radiation Measurement. Ref. 26 finds, compared with these surface observations, that irradiance in CERES-SYN1deg outperforms other satellite-derived datasets, such as the International Satellite Cloud Climatology Project Radiative Flux Data, the Global Energy and Water Exchanges Surface Radiation Budget dataset 3.0, and Modern-Era Retrospective Analysis for Research and Applications (MERRA), with substantially less average biases. Surface irradiance computed in

CERES-SYN1deg for (*i*) AS, (*ii*) CS (with aerosols, no clouds), and (*iii*) NA (no aerosol, with clouds) conditions is used to further calculate the attribution of irradiance reductions to aerosol and clouds.

Surface observations of AODs from the CARSNET are used to extensively evaluate the AODs used by CERES-SYN1deg. CARSNET is a ground-based network for observing aerosol optical properties established by the China Meteorological Administration in 2002. Between 2002 and 2013, it has gradually been expanded to 50 sites. The CARSNET AODs used here for evaluation are from ref. 39, where observations between 2002 and 2013 for each site were averaged into monthly mean data, representing the AOD climatology at each site. Cimel sun photometers are deployed for direct spectral solar radiation measurements of AODs at eight bands between 340 and 1,640 nm. CARSNET uses the same types of instruments as AERONET and applies calibrations on AOD data (40). In this study, we calculate AODs at 550 nm using the climatology of AODs at 440 nm and Angstrom exponents from CARSNET between 2002 and 2013 from Che et al. (39). We then evaluate the climatology of 550-nm AODs used in CERES-SYN1deg (2003–2013). For each site, we calculate the difference of the mean AODs ($\overline{AOD_{CERES}} - \overline{AOD_{CARSNET}}$) to represent the bias of CERES AODs vs. CARSNET; RMSEs are calculated for monthly averages for each site using

$$\sqrt{\frac{\sum_{i}^{1\le i\le 12}\left(AOD_{CERES,i} - AOD_{CARSNET,i}\right)^2}{12}},$$

where *i* stands for the month. RMSE indicates the SD of CERES AODs from the observations. Percentage bias and RMSE are acquired by simply dividing the biases and RMSEs by the $\overline{AOD_{CARSNET}}$, the mean AOD of CARSNET. Results are in *SI Appendix*, Table S3. Similar statistical analyses are also applied to the monthly mean AODs over all 50 sites together, the 4 remote sites, the 25 rural sites, and the 31 urban sites, with results shown in *SI Appendix*, Fig. S2.

Experimental Design Details. We design a total of nine experiments spanning 2003–2014 over a region (10° N to 55° N, 75° E to 145° E) covering all of China to calculate POAI (Tables 1 and 2). For each of the nine experiments, we first calculate 3-h mean POAIs for 2003–2014 incident on PV panels using CERES-SYN1deg observed irradiance data as input. For each grid cell, we then average a total of 4,383 3-h mean values into (*i*) the 2003–2014 average POAI, which we then use to calculate the average aerosol and cloud impacts; and (*ii*) 12 monthly mean POAIs to represent the monthly POAI climatology. Mean provincial and mean electricity grid values are calculated by the area weighted average of all grid cells within the provincial and grid boundaries. The 12-y average impact does not provide information on temporal variability. Therefore, we include the time series of daily mean POAI for each electricity grid in *SI Appendix*, Fig. S6, the time series of daily mean POAI changes caused by aerosols and cloud in *SI Appendix*, Fig. S7, and the quartile distributions of the time series in *SI Appendix*, Fig. S8. In this study, we focus on analyzing POAI, a more direct indicator of solar resources, assuming uniform radiation to electricity conversion efficiency for panels at different locations without relying on specific PV system types.

ACKNOWLEDGMENTS. We thank Dr. Seiji Kato and his team at NASA for providing access to and guidance on the CERES-SYN1deg dataset. Funding for this study was provided by the Andlinger Center for Energy and Environment and the Center for International Teaching and Research, both at Princeton University.

1. IEA-PVPS (2015) IEA-PVPS—trends 2015 in photovoltaic applications. Available at www.iea-pvps.org/index.php?id=92&eID=dam_frontend_push&docID=2795. Accessed July 28, 2016.
2. Goodrich AC, et al. (2013) Assessing the drivers of regional trends in solar photovoltaic manufacturing. *Energy Environ Sci* 6:2811.
3. China National Energy Administration (2015) Statistics for solar photolvoltaic electricity generation in 2015 (Beijing, China). Available at www.nea.gov.cn/2016-02/05/c_135076636.htm. Accessed July 28, 2016.
4. NEA (2016) 13th Five-year-plan (2016–2020) for solar development. Available at https://www.iea.org/media/pams/china/IEA_PAMS_China_China13thSolarEnergyDevelopmentFiveYearPlan20162020.pdf. Accessed July 28, 2016.
5. IEA (2015) *World Energy Outlook 2015* (OECD, Paris).
6. Chu J (2015) *Re100 China's Fast Track to a Renewable Future* (The Climate Group, London).
7. China National Renewable Energy Center (2014) China wind, solar and bioenergy roadmap 2050. Available at www.cnrec.org.cn/go/AttachmentDownload.aspx?id={1056eb44-8882-46a2-b4a4-c45c42d5c608}. Accessed July 28, 2016.
8. IEA (2012) *China Wind Energy Development Roadmap 2050* Available at https://www.iea.org/publications/freepublications/publication/china_wind.pdf. Accessed July 28, 2016.
9. Schmalensee R, et al. (2015) *The Future of Solar Energy* (Massachusetts Institute of Technology, Cambridge, MA).
10. Perez MJR, Fthenakis VM (2013) Long-distance interconnection as solar resource intermittency solution: Optimizing the use of energy storage and the geographic dispersion; interconnection of solar generating facilities. *Proceedings of the IEEE 39th Photovoltaic Specialists Conference (PVSC)* (IEEE, Washington, DC), pp 3367–3373.
11. Hoff T, et al. (2009) *Understanding Variability and Uncertainty of Photovoltaics for Integration with the Electric Power System* (LBNL, Berkeley, CA).
12. Streets DG, Wu Y, Chin M (2006) Two-decadal aerosol trends as a likely explanation of the global dimming/brightening transition. *Geophys Res Lett* 33:L15806.
13. Wild M (2009) Global dimming and brightening: A review. *J Geophys Res* 114:D00D16.
14. Aayog NITI (2015) Report on India's Renewable Electricity Roadmap 2030: Towards accelerated renewable electricity deployment (National Institution for Transforming India, New Delhi).
15. Wang KC, Dickinson RE, Wild M, Liang S (2012) Atmospheric impacts on climatic variability of surface incident solar radiation. *Atmos Chem Phys* 12:9581–9592.
16. Wild M, et al. (2009) Global dimming and brightening: An update beyond 2000. *J Geophys Res* 114:D00D13.
17. Xia X (2010) A closer looking at dimming and brightening in China during 1961–2005. *Ann Geophys* 28:1121–1132.
18. Wang K, Dickinson RE, Liang S (2009) Clear sky visibility has decreased over land globally from 1973 to 2007. *Science* 323:1468–1470.
19. Qian Y, Wang W, Leung LR, Kaiser DP (2007) Variability of solar radiation under cloud-free skies in China: The role of aerosols. *Geophys Res Lett* 34:L12804.
20. Persad GG, Ming Y, Ramaswamy V (2014) The role of aerosol absorption in driving clear-sky solar dimming over East Asia. *J Geophys Res Atmos* 119:10410–10424.
21. Lin C, et al. (2015) Impacts of wind stilling on solar radiation variability in China. *Sci Rep* 5:15135.
22. Zhao X, et al. (2009) Seasonal and diurnal variations of ambient PM2.5 concentration in urban and rural environments in Beijing. *Atmos Environ* 43:2893–2900.
23. Tarroja B, Mueller F, Samuelsen S (2013) Solar power variability and spatial diversification: Implications from an electric grid load balancing perspective. *Int J Energy Res* 37:1002–1016.
24. Yue M, Wang X (2015) Assessing cloud transient impacts of solar and battery energy systems on grid inertial responses. *Electr Power Compon Syst* 43:200–211.
25. Calif R, Schmitt FG, Huang Y, Soubdhan T (2013) Intermittency study of high frequency global solar radiation sequences under a tropical climate. *Sol Energy* 98:349–365.
26. Rutan DA, et al. (2015) CERES synoptic product: Methodology and validation of surface radiant flux. *J Atmos Ocean Technol* 32:1121–1143.
27. Levy RC, et al. (2010) Global evaluation of the Collection 5 MODIS dark-target aerosol products over land. *Atmos Chem Phys Atmos Chem Phys* 10:10399–10420.
28. Tao M, et al. (2015) Comparison and evaluation of the MODIS Collection 6 aerosol data in China. *J Geophys Res Atmos* 120:6992–7005.
29. Wei J, Sun L (2017) Comparison and evaluation of different MODIS aerosol optical depth products over the Beijing-Tianjin-Hebei region in China. *IEEE J Sel Top Appl Earth Obs Remote Sens* 10:835–844.
30. GEF; UNEP (2006) Solar and wind energy resource assessment (SWERA). Available at openei.org/wiki/Solar_and_Wind_Energy_Resource_Assessment_(SWERA). Accessed July 28, 2016.
31. He Q, Zhang M, Huang B, Tong X (2017) MODIS 3 km and 10 km aerosol optical depth for China: Evaluation and comparison. *Atmos Environ* 153:150–162.
32. Kvalevåg MM, Myhre G (2007) Human impact on direct and diffuse solar radiation during the industrial era. *J Clim* 20:4874–4883.
33. US Energy Information Administration (2016) *Annual Electric Generator Report* (US Energy Information Administration, Washington, DC), DOE-019-EIA-AEGR-COLL1.
34. Andrews RW, Stein JS, Hansen C, Riley D (2014) Introduction to the open source PV LIB for python Photovoltaic system modelling package. *Proceedings of the IEEE 40th Photovoltaic Specialist Conference (PVSC)* (IEEE, Washington, DC), pp 0170–0174.
35. Stein JS, Holmgren WF, Forbess J, Hansen CW (2016) PVLIB: Open source photovoltaic performance modeling functions for Matlab and python. *Proceedings of the IEEE 43rd Photovoltaic Specialists Conference* (IEEE, Washington, DC), pp 3425–3430.
36. Holmgren WF, Andrews RW, Lorenzo AT, Stein JS (2015) PVLIB python 2015. *Proceedings of the IEEE 42nd Photovoltaic Specialist Conference (PVSC)* (IEEE, Washington, DC), pp 1–5.
37. CERES Science Team (2016) CERES SYN1deg Ed3A. Available at https://eosweb.larc.nasa.gov/sites/default/files/project/ceres/quality_summaries/CERES_SYN1deg_Ed3A.pdf. Accessed July 28, 2016.
38. Doelling DR, et al. (2013) Geostationary enhanced temporal interpolation for CERES flux products. *J Atmos Ocean Technol* 30:1072–1090.
39. Che H, et al. (2015) Ground-based aerosol climatology of China: Aerosol optical depths from the China aerosol remote sensing network (CARSNET) 2002–2013. *Atmos Chem Phys* 15:7619–7652.
40. Che H, et al. (2009) Instrument calibration and aerosol optical depth validation of the China aerosol remote sensing network. *J Geophys Res* 114:D03206.
41. Landau CR (2015) Optimum tilt of solar panels. Available at www.solarpaneltilt.com/. Accessed May 18, 2016.

Reduction of solar photovoltaic resources due to air pollution in China

Supporting Information

Xiaoyuan Li[a], Fabian Wagner[b,c,d], Wei Peng[b,1], Junnan Yang[b], and Denise L. Mauzerall[a,b,2]

[a]Department of Civil and Environmental Engineering, Princeton University, Princeton, NJ 08544;

[b]Woodrow Wilson School of Public and International Affairs, Princeton University, Princeton, NJ 08544;

[c]Air Quality and Greenhouse Gases Program, International Institute for Applied Systems Analysis, A-2361 Laxenburg, Austria;

[d]Andlinger Center for Energy and the Environment, Princeton University, Princeton, NJ 08544;

Keywords: renewable energy, solar photovoltaic, aerosols, air pollution, China

[1] Present address: Belfer Center for Science and International Affairs, Harvard Kennedy School of Government, Cambridge, MA 02138.

[2] To whom correspondence should be addressed. Email: mauzeral@princeton.edu.

SI Tables

Table S1. Grid-level impact (units of kWh/m^2/day) of aerosols and clouds on point-of-array irradiance (POAI) for fixed panels (FIX). Percent impacts are calculated as the corresponding value divided by All-Sky (AS) POAI and are included in brackets.

Change of	Northern Grid	Eastern Grid	Central Grid	Northeastern Grid	Northwestern Grid	Southern Grid
Total POAI due to **Aerosols**	-0.73 (-13.7%)	-0.83 (-21.1%)	-0.62 (-15.9%)	-0.49 (-9.8%)	-0.48 (-8.6%)	-0.47 (-11.1%)
Total POAI due to **Clouds**	-1.27 (-23.8%)	-2.00 (-50.4%)	-2.34 (-59.5%)	-1.62 (-32.5%)	-1.65 (-29.6%)	-2.31 (-54.5%)
Direct POAI due to **Aerosols**	-1.17 (-38.9%)	-1.14 (-78.6%)	-0.83 (-57.7%)	-0.70 (-25.3%)	-0.91 (-30.4%)	-0.68 (-42.7%)

Table S2. Data type, descriptions and variables used for each dataset.

Dataset	Type	Description		Variables
NASA CERES -- SYN1deg Edition 3A	**Radiation**	**Spatial Resolution**	1^o by 1^o	Surface Flux of **direct**, **diffuse** and **global** **(direct + diffuse)** shortwave radiation calculated from satellite data under three atmospheric conditions: (1) **All-sky**, (2) **Clear-sky**, and (3) **All-sky-without-aerosol**.
		Temporal Resolution	3-hourly	
		Time Span	2003 - 2014	

Table S3. Location and Aerosol Optical Depth (AOD) Information from all 50 sites in the China Aerosol Remote Sensing Network (CARSNET) and results for the statistical comparison with AOD climatology from CERES-SYN1deg.

Site	Location			AOD_{CERES}	$AOD_{CARSNET}$	Bias		Root-Mean-Square Error	
	Lon.	Lat.	Alt. (m)	Mean	Mean	Mean	%		%
Remote Sites (4 sites)									
Akedala	47.12	87.97	562	0.195	0.154	0.041	26.58	0.111	71.62
Lhasa	29.67	91.13	3663	0.137	0.094	0.043	45.55	0.088	93.73
Mt. Waliguan	36.28	100.92	3810	0.239	0.128	0.111	86.78	0.147	115.34
Shangri-La	28.02	99.73	3583	0.174	0.083	0.092	110.84	0.112	135.14
Rural Sites (24 sites)									
Dunhuang	40.15	94.68	1139	0.256	0.293	-0.037	-12.68	0.196	66.93
Ejina	41.95	101.07	940.5	0.244	0.221	0.023	10.51	0.152	68.72
Hami	42.82	93.52	737	0.226	0.221	0.004	1.98	0.151	68.48
Hotan	37.13	79.93	1374.7	0.501	0.591	-0.090	-15.31	0.184	31.12
Jiuquan	39.77	98.48	1477.3	0.287	0.277	0.010	3.73	0.187	67.72
Minqin	38.63	103.08	1367	0.308	0.344	-0.036	-10.40	0.134	38.80
Tazhong	39	83.67	1099.4	0.258	0.512	-0.254	-49.57	0.323	63.15
Wulate	41.57	108.52	1288	0.300	0.240	0.060	24.95	0.156	65.03
Xilinhot	43.95	116.12	1003	0.212	0.217	-0.005	-2.42	0.072	32.90
Zhangbei	41.15	114.7	1093.4	0.280	0.268	0.012	4.35	0.089	33.36
Zhurihe	42.4	112.9	1152	0.215	0.203	0.012	6.07	0.072	35.61
Dongsheng	39.83	109.98	1460.5	0.318	0.382	-0.064	-16.76	0.107	28.11
Mt. Gaolan	36	103.85	2161.6	0.392	0.390	0.001	0.33	0.175	44.78
Yan'an	36.6	109.5	958.5	0.402	0.308	0.094	30.56	0.139	45.21
Yulin	38.43	109.2	1135	0.343	0.318	0.026	8.09	0.125	39.27
Changde	29.17	111.7	565	0.929	0.455	0.474	104.33	0.490	107.86
Dongtan	31.52	121.96	10	0.816	0.479	0.336	70.24	0.361	75.30
Gucheng	39.13	115.8	45.2	0.566	0.534	0.032	5.89	0.197	36.81
Huimin	37.48	117.53	11.7	0.851	0.554	0.297	53.59	0.358	64.58
Lin'an	30.3	119.73	138.6	0.657	0.587	0.070	11.91	0.129	21.96
Mt. Longfeng	44.73	127.6	330.5	0.326	0.246	0.080	32.40	0.151	61.09

Mt. Tai	36.25	117.1	1591	0.774	0.249	0.525	210.75	0.535	214.84
Shangdianzi	40.65	117.12	293	0.430	0.377	0.053	14.01	0.153	40.44
Tongyu	44.42	122.87	151	0.308	0.196	0.111	56.69	0.156	79.30
Yushe	37.07	112.98	1041.5	0.559	0.457	0.103	22.48	0.174	38.21
Urban sites (31 sites)									
Anshan	41.08	123	23	0.520	0.587	-0.067	-11.37	0.171	29.21
Beijing	39.8	116.47	31.3	0.732	0.605	0.127	21.02	0.261	43.07
Benxi	41.32	123.78	183	0.520	0.760	-0.240	-31.58	0.222	29.23
Chengdu	30.65	104.03	496	0.930	0.768	0.162	21.11	0.238	31.01
Dalian	38.9	121.63	91.5	0.591	0.421	0.171	40.56	0.209	49.77
Datong	40.1	113.33	1067.3	0.324	0.419	-0.096	-22.79	0.160	38.24
Fushu	41.88	123.95	80	0.520	0.437	0.083	19.02	0.254	58.07
Hangzhou	30.23	120.17	42	0.854	0.803	0.051	6.34	0.143	17.77
Hefei	31.98	116.38	92	0.801	0.686	0.115	16.78	0.184	26.82
Kunming	25.01	102.65	1889	0.380	0.363	0.016	4.53	0.100	27.59
Lanzhou	36.05	103.88	1517.3	0.392	0.663	-0.272	-40.94	0.385	58.00
Nanjing	32.05	118.77	99.3	0.832	0.718	0.114	15.84	0.199	27.65
Nanning	22.82	108.35	172	0.643	0.678	-0.035	-5.12	0.093	13.74
Panyu	23	113.35	145	0.705	0.644	0.061	9.43	0.166	25.69
Pudong	31.22	121.55	14	0.816	0.663	0.153	23.01	0.203	30.63
Shenyang	41.77	123.5	60	0.520	0.632	-0.112	-17.68	0.189	29.94
Tianjin	39.1	117.17	3.3	0.748	0.627	0.121	19.30	0.215	34.24
Urumqi	43.78	87.62	935	0.267	0.415	-0.148	-35.67	0.310	74.77
Xi'an	34.43	108.97	363	0.718	0.734	-0.016	-2.20	0.104	14.14
Yinchuan	38.48	106.22	1111.5	0.380	0.460	-0.080	-17.33	0.219	47.55
Zhengzhou	34.78	113.68	99	0.934	0.759	0.175	23.13	0.242	31.85

SI Figures

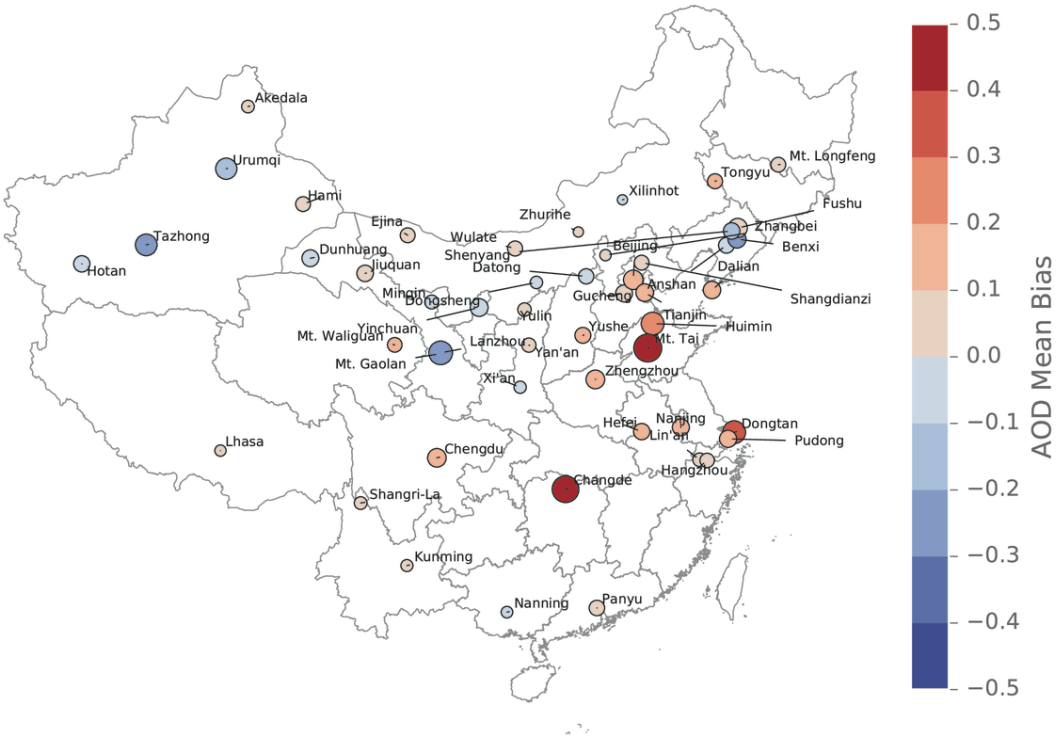

Figure S1. Comparison between AOD monthly climatology used for CERES-SYN1deg and observations from CARSNET at 50 sites in China from 2003-2014. Color represents the mean bias: CERES minus CARSNET. Root-mean-square error (RMSE) is indicated by the size of the circles. Values of biases, RMSEs, percent error, as well as the site information, are shown in Table S3.

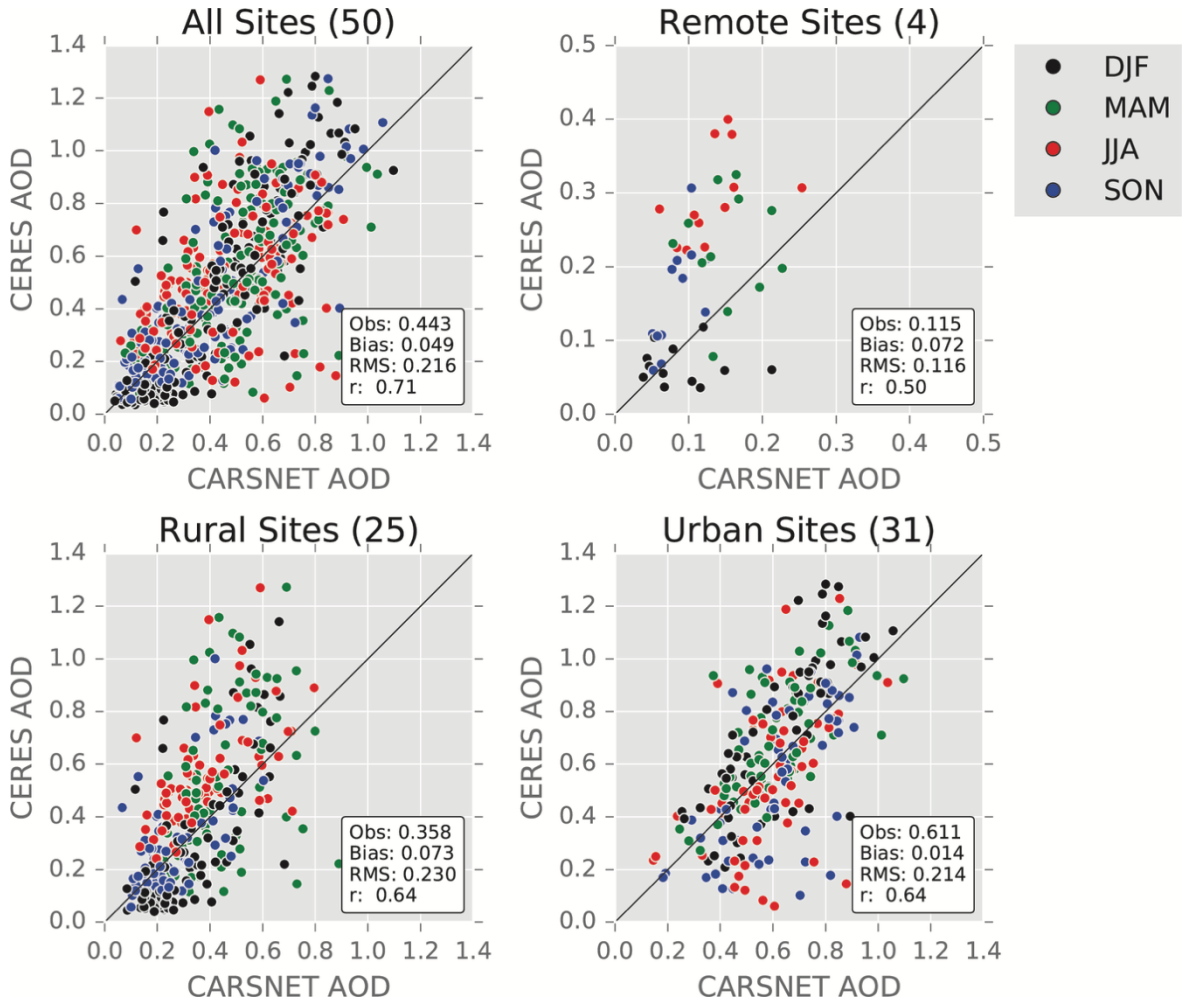

Figure S2. Comparison of monthly-mean AOD climatology between CERES-SYN1deg (2003-2014) and CARSNET (2002-2013, only available for 12-year average without data for individual years) at all 50 sites (upper left), and re-grouped into remote sites (upper right), 25 rural sites (lower left), and 31 urban sites (lower right). Each color represents mean values for a season: black marks denote December, January and February (DFJ), green marks denote March, April and May (MAM), red marks denote June, July and August (JJA), and blue marks denote September, October and November (SON). Observational mean (Obs), mean bias (Bias), root-mean-square error (RMS) and correlation coefficient (r) for each category are shown in the box.

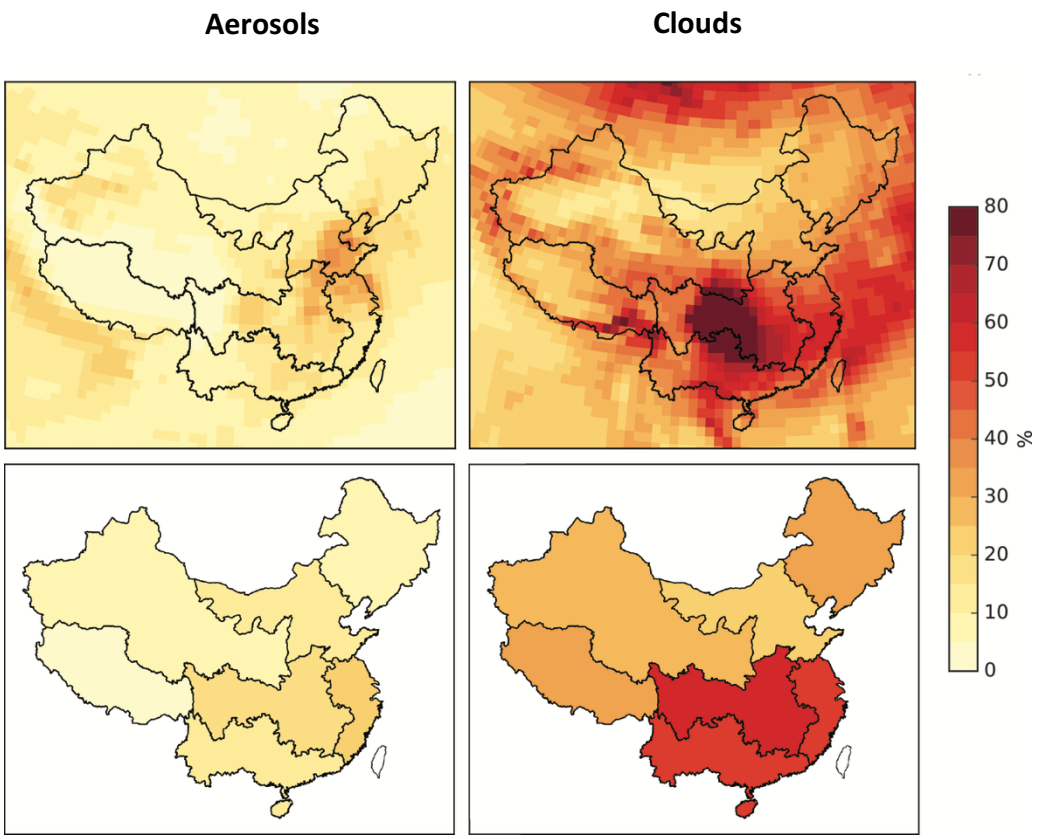

Figure S3. % Reduction of Point-of-Array Irradiance due to Aerosols and Clouds at 1° x 1° grid-cell level (upper panels) and for each electricity grid (bottom panels). Values of grid-level reduction can be found in Table S1.

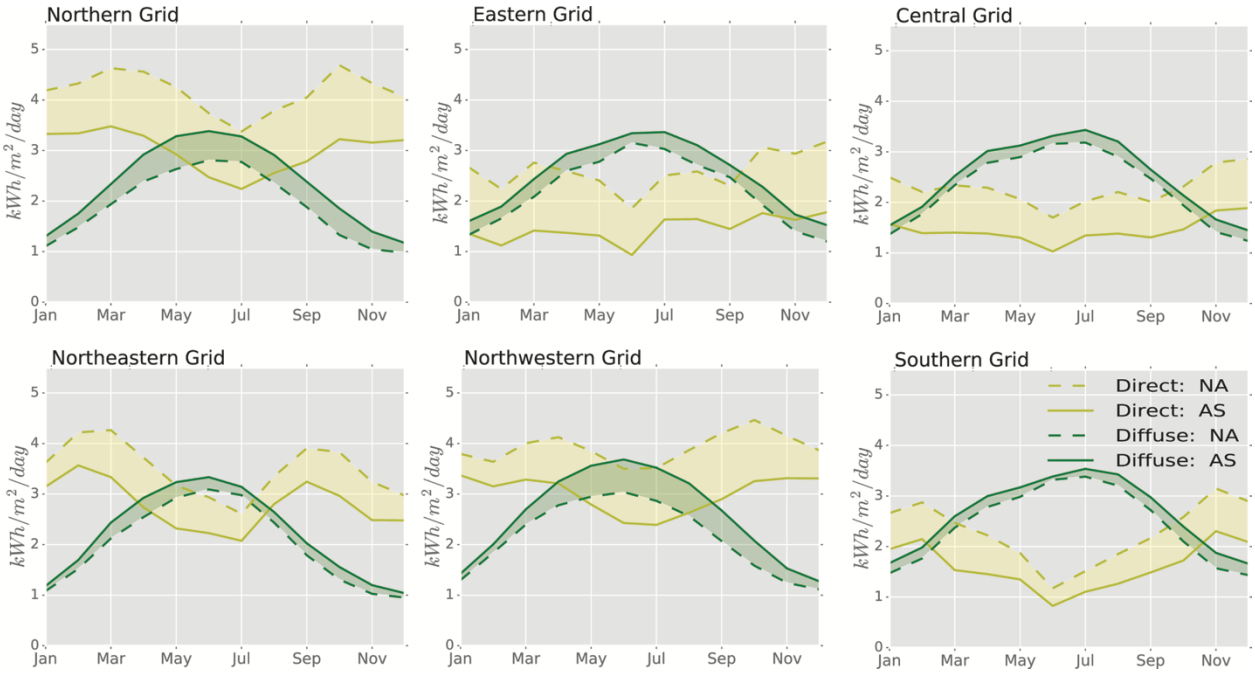

Figure S4. Seasonality of Point-of-Array Direct and Diffuse Irradiance for China's Six Electricity Grids.

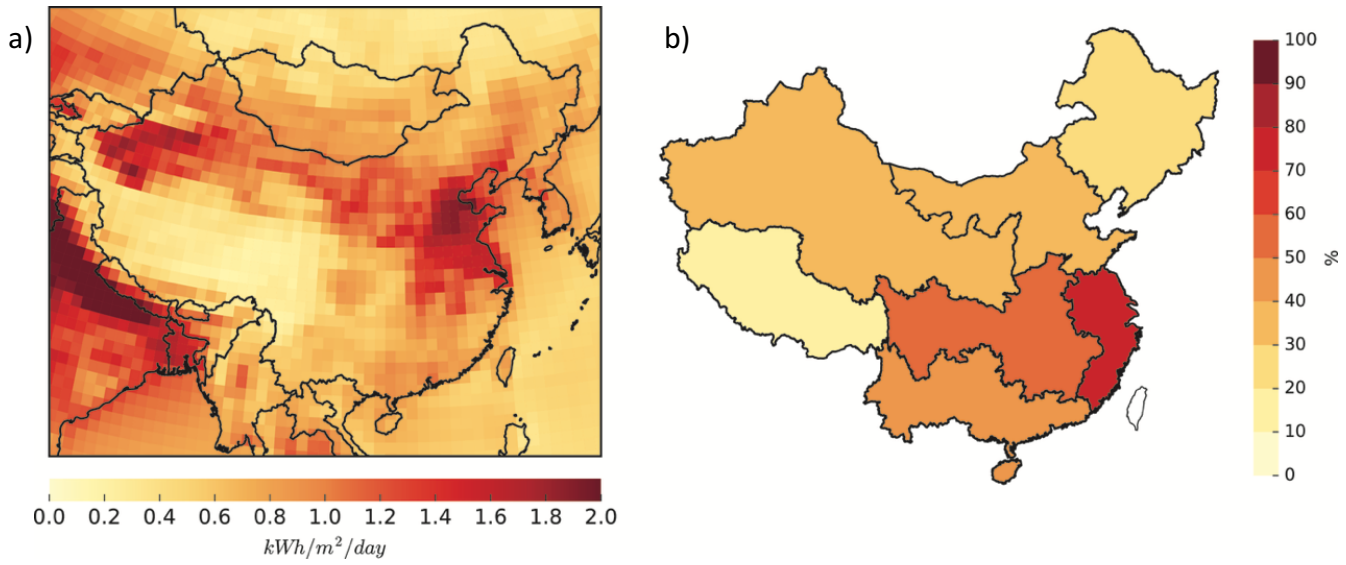

Figure S5. Reduction of Point-of-Array surface direct radiation due to aerosols: a) absolute loss; b) percentage loss. Values of grid-level reduction can be found in Table S1.

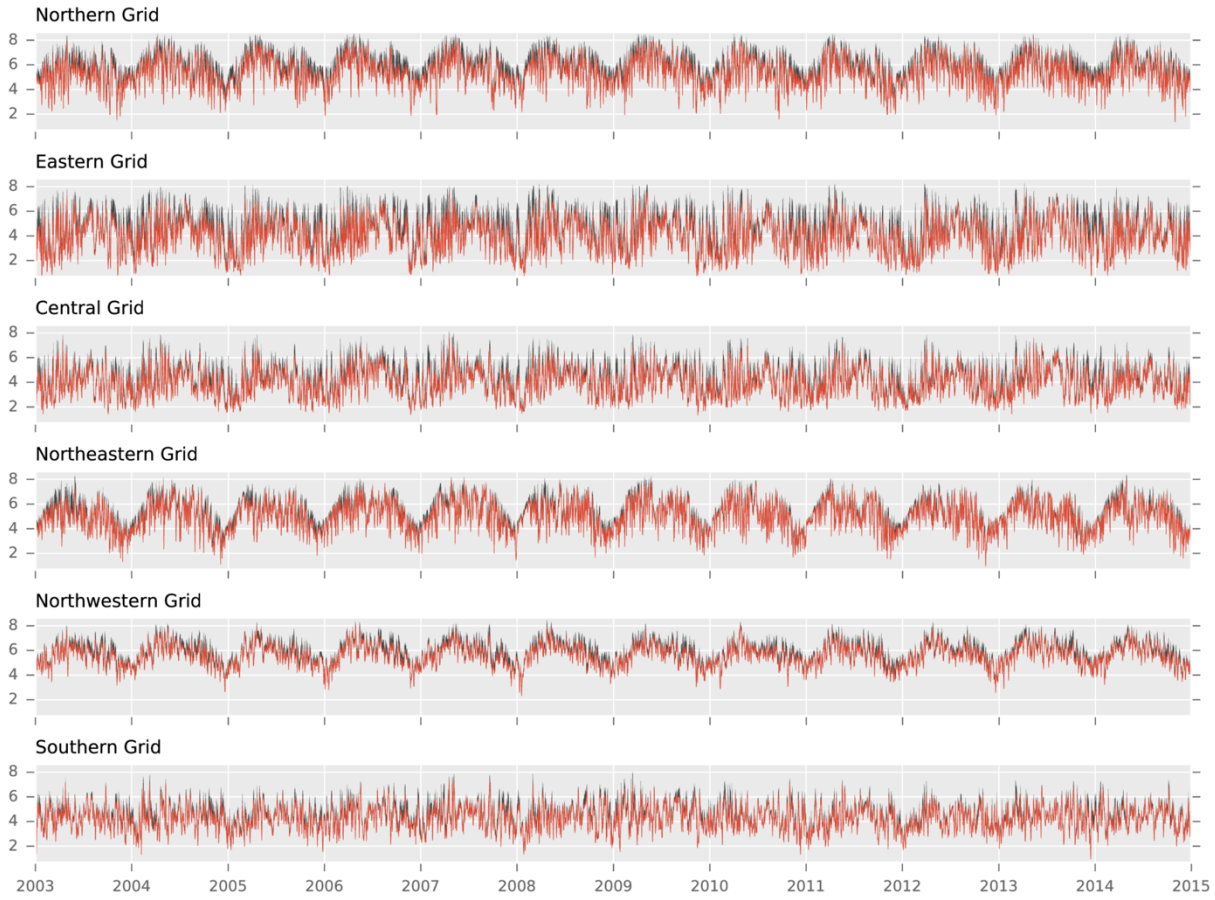

Figure S6. Time series of daily-mean point-of-array-irradiance for fixed panels averaged over each electricity grid in China. The red lines represent the All-sky scenario. The black lines represent the All-sky-without-aerosol scenario. The variability is primarily driven by clouds as can be seen by the similarity between the red and black lines. The black shaded areas indicate the aerosol impacts (allowing detection of heavy aerosol episodes by thicker shading). Units are $kWh/m^2/day$.

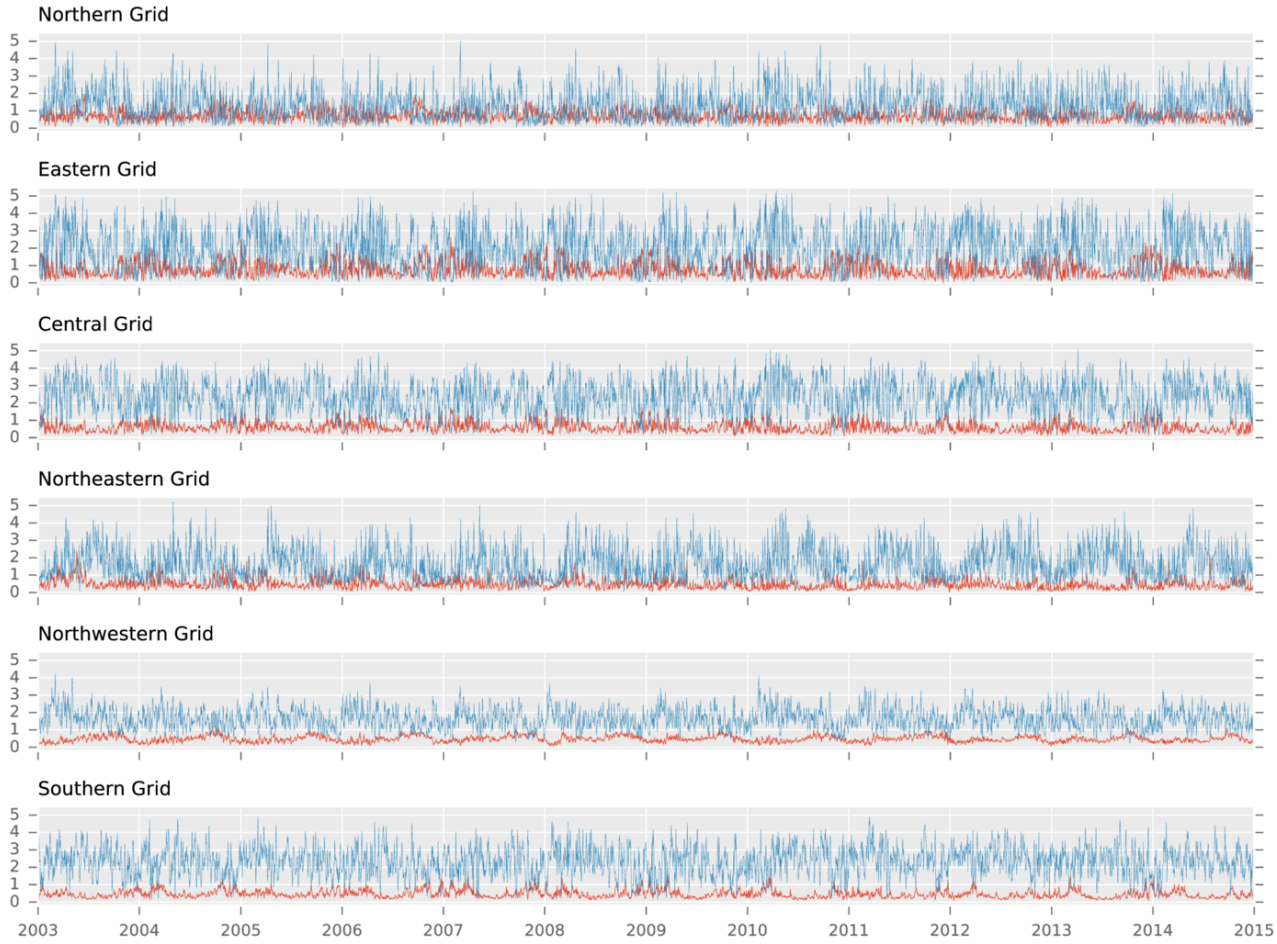

Figure S7. Time series of daily-mean point-of-array-irradiance changes due to aerosols (red) and clouds (blue) for fixed panels averaged over each electricity grid in China. The red lines represent the aerosol impacts. The blue lines represent the cloud impacts. The variability of aerosol impacts is much less than that of clouds. Units are kWh/m^2/day.

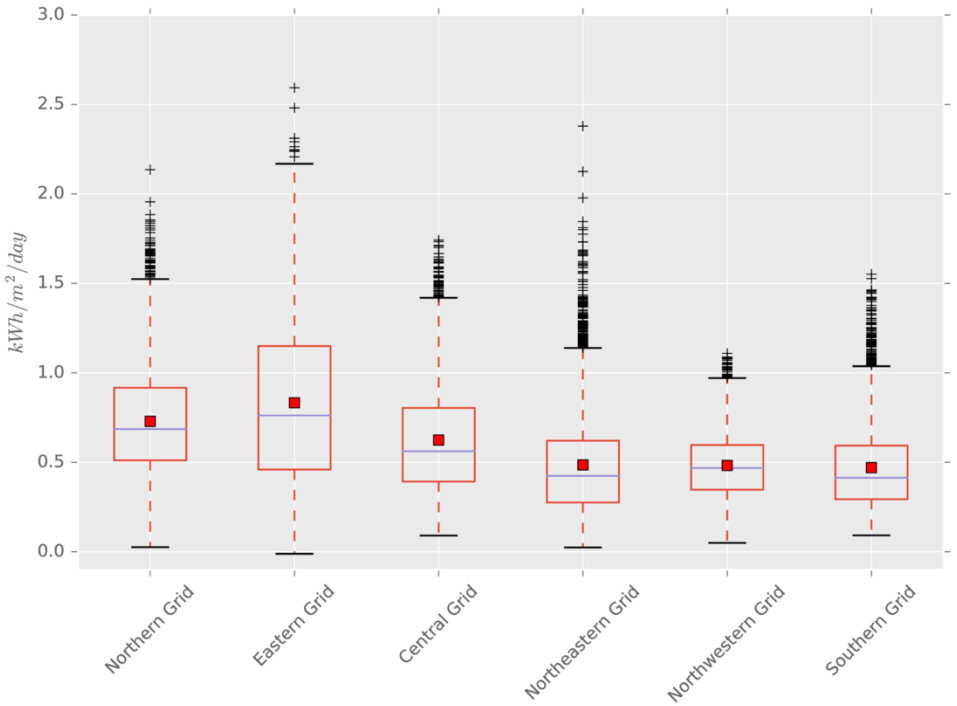

Figure S8. Boxplots of daily-mean aerosol impacts on the point-of-array-irradiance for fixed panels for each electricity grid in China. These are standard statistical boxplots. Each box extends from the first quartile (Q1) to the third quartile (Q3) values of the data, with a line at the median. Where IQR is the interquartile range (Q3-Q1), the upper whisker extends to the last datum less than Q3 + 1.5×IQR. Similarly, the lower whisker will extend to the first datum greater than Q1 – 1.5×IQR. Beyond the whiskers, data are considered outliers and are plotted as individual points. Red squares represent mean values.